Eur. Phys. J. B **56**, 311–322 (2007)
DOI: 10.1140/epjb/e2007-00137-0

THE EUROPEAN PHYSICAL JOURNAL B

Size selected growth of nanodots: effects of growth kinetics and energetics on the formation of stationary size distributions

K.A. Nevalainen[1,a], M. Rusanen[1,2], and I.T. Koponen[2]

[1] Laboratory of Physics, Helsinki University of Technology, P.O. Box 1100, 02015 TKK, Finland
[2] Department of Physical Sciences, P.O. Box 64, 00014 University of Helsinki, Finland

Received 15 February 2007 / Received in final form 11 April 2007
Published online 16 May 2007 –

Abstract. The size selection of nanodots during the growth is studied by using a reaction kinetic model, where reaction rates depend on the dot size. The characteristic feature of the reaction rates is the energetics, where the free energy of dots has a minimum at the certain dot size. The model equations are solved by using a particle coalescence simulation method. We find phenomenologically three distinct stages of growth. First, during the initial deposition stage, distributions with high density of small dots occur. Second, there is an intermediate and short-lived stationary state, which is controlled by kinetics of growth. Third, a long-lived stationary state is obtained, with nearly Gaussian size distributions, mostly determined by the energetics of the growth but also significantly affected by the kinetics. In the final stage, size selection and narrowing of the distributions occur. It is also shown that in the final stage of growth the Fokker-Planck type continuum model describes well the evolution of the distributions and the size selection.

PACS. 81.07.Ta Quantum dots – 68.65.Hb Quantum dots – 68.35.Md Surface thermodynamics, surface energies – 81.16.Dn Self-assembly

1 Introduction

In growth of nanosized clusters and dots on surfaces there are interesting cases, where size-selection of dots take place [1–6]. The size-selected growth has given promises to realize in practical situations the self-assembled production of regular sized arrays of nanodots [7,8]. The spontaneous size-selection is known to occur in 2D-growth of nanodots, when growth proceeds in the Stranski-Krastanov mode with a wetting layer [5], and also in the 3D-growth of nanoclusters proceeding in the Volmer-Weber mode, characterized by immediate cluster formation [3,4,6]. In most cases size selection is observed in heteroepitaxy of semiconductor nanodots, but also in heteroepitaxy of metallic dots [5,6,9–11].

The physical origin of size-selection is often ascribed to the thermodynamics of growth and the existence of energy minimum for the dot formation energy per atom. In 2D heteroepitaxial growth the existence of such minimum can be related to the elastic relaxation energy due to misfit strain [12–14] and in 3D growth to the surface energy and on its dependence on the morphology of the clusters [6,15]. In the case of thermodynamically driven growth the equilibrium distribution is the Gibbs-Boltzmann distribution corresponding the thermodynamically stable state, and the optimum size is determined by the minimum of the formation energy [2,16].

Another possibility is to attribute the size selection to the reaction kinetics, where basic atomistic processes of growth, the attachment and detachment to cluster edges, are all processes depending on the size of the nanoclusters [12,13,17,18]. In both cases, however, the size selection is connected to the minimum of total energy of the growing structures with respect to their size. The major difference of the views based on thermodynamic and kinetic descriptions is on the role of growth kinetics determining the form of the stationary distribution. The thermodynamic description relates the size selection to the stable Gibbs-Boltzmann distribution, whereas the kinetic description relates it to the long-lived, metastable distribution which results from the interplay between energetics and the kinetics of growth. The optimum size in kinetic description is no more simply related to the minimum of the formation energy [12–14,17,18].

The kinetically determined metastable state and size selection has been studied in several previous works. The kinetically determined size selection has been demonstrated in simulations [5,12,13], in closely related phenomenological continuum models [14], and in fully kinetic descriptions in terms of reaction rates of adatom attachment and detachment processes [17,18]. Moreover, the transition from kinetically controlled to

[a] e-mail: kirsi.nevalainen@gmail.com

thermodynamically driven growth can be seen in cases, where the effects of size dependent energetics are taken into account directly through the microscopic rates governing the growth [12,13]. In summary, the results of the studies, which are explicitly based on microscopic descriptions, support the view that the size selection is a generic feature of growth. Size selection is related to the existence of long lived metastable state, where evolution of the distribution is affected by both the energetics and kinetics of the growth [12–14]. In such cases, the selected size may significantly exceed the size corresponding to the energy minimum [14].

The size selection of nanodots occurring due to combined effects of energetics and kinetics of growth has recently been discussed in terms of Fokker-Planck model. The advantage of such description is that it makes a direct connection to kinetic models of growth, and it is possible to obtain the Fokker-Planck model from the underlying reaction kinetic Becker-Döring model [14]. The results based on the Fokker-Planck model show that the time evolution of the size distribution for size selected nanodots is Gaussian-shaped, and the system evolves steadily towards the long-lived metastable state. Already before the metastable state is reached, the width of the size distribution begins to diminish, and in the stationary state it is at its narrowest. The possibility to obtain the time evolution of the size distribution in terms of Gaussian distribution is somewhat unexpected, because the cluster growth even in simple reversible cases usually leads to more complicated distributions of scaling form.

In this work, we examine the size selected growth of nanodots by using a reaction kinetic model (RKM) with self-consistent reaction rates for size dependent attachment and detachment processes. The energetics of the adatom process is described through the free energy difference of the growing dots. In continuum limit, this quantity is equal to the chemical potential. The growth as governed by the RKM is then simulated numerically by using the particle coalescence method (PCM), which we have previously developed [19] for similar reaction kinetic growth problems. This approach allows us to study in detail the evolution of the size distribution function in all stages of the growth. The results show that there are three characteristic stages, namely (1) the initial stage, with high density of small dots (singular distribution); (2) intermediate stage of short-lived stationary state corresponding the minimum of the detachment rate, strongly ordinated by growth kinetics; and (3) final long-lived stationary state mostly dictated by the energetics of the growth, but still displaying a significant overshooting effect due to the kinetics.

2 The reaction kinetic model of size selected growth

The nanodot growth is described by the reaction kinetic model (RKM), which includes only adatom attachment and detachment processes $A_1 + A_s \leftrightarrow A_{1+s}$ with dots of size s. The reaction rates for attachment and detachment σ_s and γ_s, respectively, are specified later. This model simplifies the real growth problem by ignoring all spatial correlations between the dots, only the average effect of dot density is taken into account through the energetics of the growth. The rate equations (RE) for adatom and dot densities n_1 and n_s corresponding the RKM are

$$\frac{dn_1}{dt} = \Phi - 2\sigma_1 n_1^2 - n_1 \sum_{s\geq 2} \sigma_s n_s + 2\kappa\gamma_2 n_2 + \sum_{s\geq 2} \kappa\gamma_s n_s;$$

$$\frac{dn_s}{dt} = \sigma_{s-1} n_{s-1} n_1 - \sigma_s n_s n_1 + \kappa\gamma_{s+1} n_{s+1} - \kappa\gamma_s n_s, \quad (1)$$

where t is time, Φ is the deposition flux of adatoms in monolayers (ML) per second, $\theta = \Phi t$ is the coverage in MLs. The parameter κ defines the total rate $\kappa \sum \gamma_s n_s$ of detachment events (per site). We are mostly interested in the region, where the adatom density becomes stationary and $dn_1/dt = 0$. Then size distributions are of shape preserving form and become also independent of parameter κ and adatom density n_1. From equation (1) it is seen that this condition is fulfilled when $n_1 \to \kappa$. Moreover, then the total rate of detachment events becomes equal to total rate $n_1 \sum \sigma_s n_s$ of attachment events. In this limit, classical Becker-Döring description of the growth is obtained (Appendix B). However, the prediction of the time needed to obtain the full stationarity of growth with $n_1 = \kappa$ is difficult to estimate and therefore in what follows we use the full RE description.

2.1 The reaction rates

In systems, where size selection takes place, the reaction rates have energy barriers depending on the dot size. There are several possibilities for the physical origin of the dot size dependent energetics, but the essential feature of the energetics is the existence of the minimum value for energy difference $\Delta_s = E_{s+1} - E_s$, where E_s is the total free energy of dot of size s. The form to be used for the free energy difference Δ_s is specified later. The transition rates σ_s and γ_s can be then defined in terms of the effective energy barriers Δ_s, with an additional requirement that for reversible processes $A_1 + A_s \leftrightarrow A_{1+s}$ the reaction rates for attachment and detachment need to fulfill the condition of detailed balance

$$\frac{\gamma_{s+1}}{\sigma_s} = e^{\beta\Delta_s}. \quad (2)$$

However, apart from the requirement of detailed balance there are more freedom how to define the rates. In different models of nucleation and growth the free energy for transition is divided differently between the effective barriers for attachment and detachment. For example, in the widely used Turnbull-Fisher model and Kelton-Greer model based on it, the free energy is divided symmetrically [20,21], but in some models the free energy is taken into account either in the attachment or detachment barrier only (see Ref. [22]).

In the present case, the most obvious choice for defining the detachment and attachment barriers is to follow the self consistent scheme introduced by Bales and Zangwill [23], which leads to reaction rates (see Appendix A),

$$\sigma_s = s^q/(1+e^{\beta\Delta_s})$$
$$\gamma_s = s^q/(1+e^{-\beta\Delta_{s-1}}). \quad (3)$$

where $\beta = 1/k_BT$ is the inverse temperature. In these reaction rates, the prefactor s^q takes into account the geometric size dependence of the reaction rates, simply related to the length of the dot boundary. The parameter q is thus related to the morphology of the growing dots, and because we are mostly concerned with 2D compact dots $q = 1/2$ is an appropriate choice. However, because of size dependence of prefectors of reaction rates, some 2D cases may be better described with values ranging from $1/4 < q < 2/3$. The reaction rates in equation (3) fulfill the condition of detailed balance, and in the limit of large barriers and low temperatures where $-\beta\Delta_s \gg 1$ the rates in equation (3) agree with rates in Turnbull-Fisher and Kelton-Greer models [20,21]. The self-consistent detachment rates at three different temperatures are shown in Figure 1. The current choice of barriers gives very low attachment rates at small dot sizes. There is a critical size of dots, corresponding to the saddle point of detachment rates seen in Figure 1, which needs to be overcome before growth proceeds rapidly. In practice, in the region of sizes smaller than the critical size, deposition defines the timescale needed to reach the critical size. In order to speed up the evolution in this region we approximate the attachment rate with a simple power-law form $\sigma_s \to s^q$. This approximation agrees with the self-consistent rates in region of dot sizes exceeding the critical size, but simplifies the description in the region of attachment limited growth at sizes smaller than the critical size. Therefore, in our model the initial stage of growth is essentially the reversible growth process governed by power-law type reaction rates.

2.2 Energetics of growth

The energetics of the model is defined through the total free energy E_s of the dot of size s. In many previous studies on the size selection the free energy is based on expression suggested by Tersoff and Tromp [24], which takes into account the effects of the elastic strain field around the growing dot. However, there are situations where the Tersoff-Tromp energetics is not successful, in particular in case of metallic nanodots [6,9,25]. In case of metallic dots the total "self-energy" of the dot can be represented as a combination of power-law type of terms of the form s^α (with $\alpha > 0$), and in addition to these, contributions from dot-dot interactions and possibly also from the Gibbs-Thomson effect, which both can be included in an inverse power-law term $s^{-1/2}$ [24,26]. In what follows, we will use a simpler, phenomenological form introduced by Gai et al. [6], which is in agreement with theoretically more motivated but also more complicated expression suggested by Liu [9]. This choice leads to free energy difference of the form

$$\Delta_s = w_0 + c\, s^\alpha + a\, s^{-p}. \quad (4)$$

In the case of non-strained metallic dots, where self-assembly and size selection are driven by coverage-dependent dot-dot interactions, the first term describes the "self-energy" of dots, including e.g. strain energy, interface energy and step energy, while the latter term with $a = g\theta^{2/3}$ describes the coverage-dependent dot-dot interaction with interaction strength g [6,9]. The parameter w_0 is the constant part of self energy, which sets the minimum value of the total free energy. In fact, with suitably chosen set of parameters also the Tersoff-Tromp type energetics for strain field driven self-assembly can be represented by equation (4). It should be noted, that the energy difference Δ_s describes the energy needed to remove or add one atom to the dot of size s, and in the continuum limit it corresponds to the the chemical potential $\mu(s) = \partial E(s)/\partial s$ of dot of size s. Therefore, in the limit of very large islands our description is consistent with the continuum description of the self-assembled growth process [14]. In the following we do not explicitly discuss the effect of coverage on the self-assembly, but rather use equation (4) as a convenient and flexible fitting formula for several possible types of energetics of different physical origin. Nevertheless, we need to define the basic energy scale for the further reference. Towards this end we note that the minimum energy Δ_{min} should represent the energy needed to remove one atom from the most stable configuration (i.e. energy of at least one dangling bond), and for this energy values in range 0.2–0.4 eV are appropriate [2,17,18]. In addition, the temperature scale depends also on the choice of the energy scale, because what matters is the dimensionless value of $\beta\Delta_{min}$. Therefore, it is convenient to make the following scaling $\beta \to a\beta$, $c \to c/a$ and $w_0 \to w_0/a$ and set $a \to 1$ thus reducing the number of free parameters. With this choice we mostly use parameterization where minimum energy becomes $\Delta_{min} = -0.25$ eV, corresponding size $s_0 = 5000$ and temperatures in range 70 K–700 K as mentioned in results given further on. Different energy and temperature scales are obtained by different choice of a so that $T \to aT$ and $\Delta_{min} \to a\Delta_{min}$.

2.3 Simulations

The rate equations (1) are solved by numerical simulation of the time development of distributions by using the particle coalescence method (PCM) [19,27,28]. In the PCM, the configuration space of dots is sampled, and the most probable reactions are realized with weights given by the rates. For the stochastic sampling, an efficient algorithm is needed. The simplest and most efficient algorithm in simulations of non-equilibrium systems like the current one, is the rejection-free Bortz-Kalos-Lebowitz (BKL) algorithm [29]. The use of BKL provides us with possibility to obtain large amounts of data of good quality in very

reasonable computing times. In the PCM it is assumed that all dots can be treated as point-like objects, implying a low-coverage limit.

At every time step of simulation a dot process (attachment, detachment or deposition if included) is picked up according to pre-determined probability calculated from the rates and the instantaneous dot distributions. In case of deposition, an extra adatom is simply added. The probabilities needed to choose processes are stored in a binary tree to fasten the searches and updates of new, changed probabilities during simulations. In order to keep track of the time, the length of time step is calculated from the total rate of events. A more detailed description of the method and of its implantation are given in our previous work [19].

3 Results

The results of the PCM simulations demonstrate the existence of the three phenomenologically different growth stages of nanodots: (1) the initial stage during deposition, with high density of small dots (singular growth), and after the deposition is interrupted; (2) intermediate stage of short-lived stationary growth, which occurs at the minimum of detachment rate and is strongly ordinated by the kinetics of the growth; and (3) final long-lived stationary state mostly governed by energetics of the growth, but displaying a significant overshooting effect due to the kinetics. The results discussed here illustrate the generic behaviour of systems, where metastable kinetic states with stationary size distributions occur. The simulations with different parameters for energetics do not correspond any specific real system, although by suitable choice of parameters different real systems can be modelled.

3.1 Initial evolution of the singular distributions

The initial distribution of the nanodots is prepared by deposition of adatoms, and therefore the initial evolution of the size distribution is governed by the deposition flux and the reaction rates, which have essentially only the size dependence of the type s^q, as is shown Figure 1. In the absence of the size-dependent energetics of the detachment rates, the growth is a kinetically determined reversible growth process, and we may expect that the size distributions in this regime have a scaling form $n_s(\theta) = \theta\langle s\rangle^{-2} f(s/\bar{s})$, where $x = s/\langle s\rangle$, $\langle s\rangle$ is the average dot size, and $f(x)$ is the scaling function (for details, see Refs. [19,30]). At high temperatures, the size dependent energetics modifies the behaviour in this region, but at low enough temperature region the evolution of the scaling form of the size distribution of the small islands is expected. The behaviour of $\langle s\rangle$ and the total nanodot density $N = \sum n_s$ are shown in Figure 2, and the scaled dot size distribution in Figure 3. From these results it is seen that the average size and total density of dots have close resemblance to the power-law type dynamic scaling laws, but the region where this kind of scaling occurs is too limited

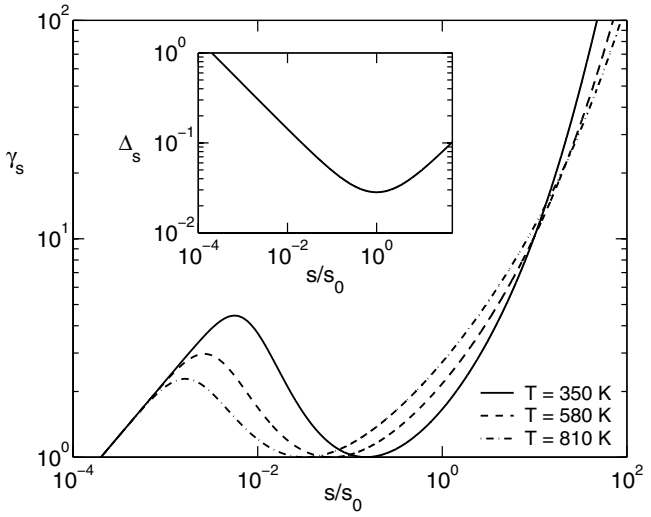

Fig. 1. The detachment rates γ_s as a function of dot size s/s_0 at three different temperatures $\beta^{-1} = 0.03, 0.05$ and 0.07, corresponding to $T = 350$, 580 and 810 K. Parameters defining the energetics are $c = 0.0002$ and $\alpha = 0.5$. The minimum values of rates are at sizes $0.15s_0$, $0.06s_0$ and $0.03s_0$, where $s_0 = 5000$. In the inset is the free energy difference Δ_s which has a minimum at s_0.

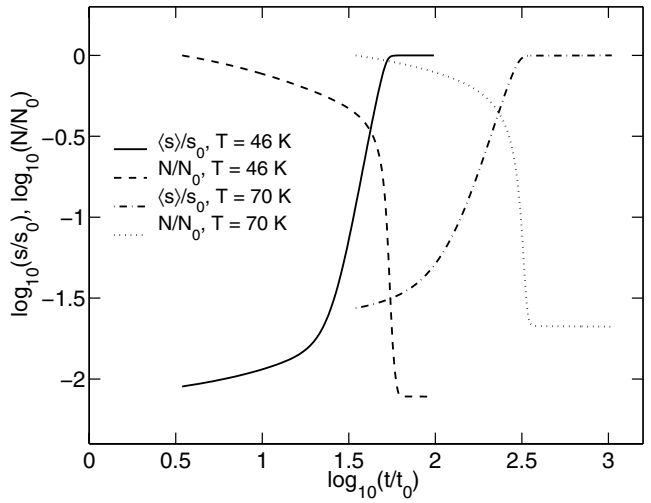

Fig. 2. The average size $\langle s\rangle/s_0$ and the total dot density N/N_0 as a function of scaled time t/t_0 in the initial stages of growth with $q = 1/2$. Note that in this figure the parameters $s_0 \approx 1350$, $t_0 \approx 10$ at $T = 70$ K and $s_0 \approx 4090$, $t_0 \approx 160$ at $T = 46$ K (other parameters are $c = 0.0002$ and $\alpha = 1/2$). The errors are within the width of lines.

for the accurate determination of the scaling exponents. The size distribution of the dots also has inverse power-law singularity at small sizes, which is apparently determined by the value of the model parameter q. These results can be understood simply as the initial evolution stage of the strongly reversible growth region. This region of growth is discussed in Appendix B in terms of Becker-Döring model, and it is shown that in the continuum limit the evolution of the size distribution is described by the non-linear

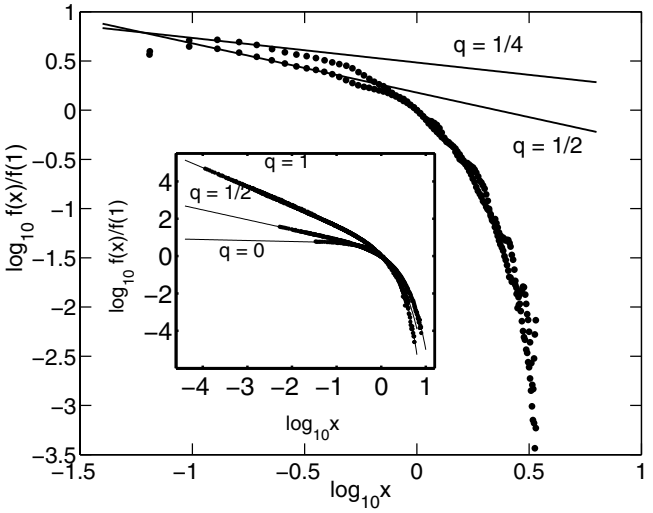

Fig. 3. The scaled initial singular distribution $f(x)/f(1)$ as a function of size $x = s/\langle s \rangle$. Figure contains data sets with two different values for the kinetic exponent q (at $T = 70$ K, $c = 0.0002$ and $\alpha = 1/2$). The inset shows the reversible growth results from longer simulations. The error bars are smaller than the symbol sizes.

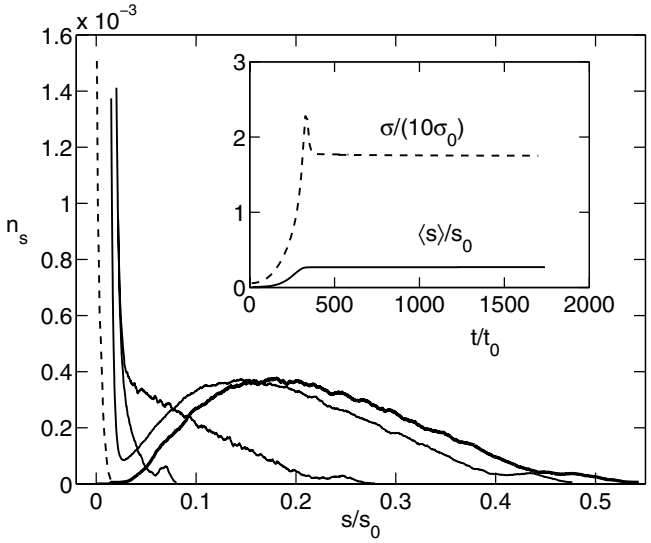

Fig. 4. The size distribution n_s as a function of size s/s_0 in the intermediate stationary stage of growth. The stationary state is determined by the minimum of the detachment rate, which occurs with current parameters at $0.27s_0$. Note the difference compared to the minimum $s_0 = 5000$ of energy function Δ_s in equation (4) (see inset of Fig. 1). The distributions are taken at times 20, 600, 2000, 3200 and 10 000 in arbitrary units and multiplied for clarity with the factors $1, 500, 500, 1000$ and 1100, respectively. Temperature is 70 K, and other parameters are $\alpha = q = 0.5, \kappa = 10^{-7}$, $c = 0.0002$, $\sigma_0 \approx 30$, and $t_0 \approx 10$.

diffusion equation, which has a solution $n(s, \theta) \propto s^{-q}$. For a better comparison of these results, simulation results of an idealized situation of reversible growth with $\sigma_s = \gamma_s = s^q$ and in regular region with $n_1 = \kappa$ are shown in the inset in Figure 3 for $q = 0, 1/2$ and 1. These results show the initial distributions obtained by the deposition are strongly singular ones, where the singularity s^{-q} at small sizes is determined by the size-dependent reaction kinetic factors of the form s^q. However, with increasing temperature the form of the distribution becomes less regular, although the peaked shape is still retained at high temperatures.

3.2 Intermediate stage of growth determined by reaction kinetics

The attachment and detachment rates have a power-law s^q-behaviour at small sizes up to a certain critical size s_{crit} defined by a temperature-dependent local maximum of the detachment rate (see Fig. 1). In the simulations, deposition is interrupted after the critical size is reached and the growth proceeds as driven by the reaction kinetics alone. The size distribution then begins to change to a propagating Gaussian distribution, as is shown in Figure 4. At the same time, the singularity of small dots starts to disappear. During the further evolution, the singularity disappears altogether, and at high enough temperatures the evolution proceeds towards the minimum of the free energy. However, at temperatures low enough with respect to the energetics, the Gaussian-shaped distribution attains a temporary stationary state before the free energy minimum. This stationary location of the distribution corresponds the minimum of reaction rates shown in Figure 1, and is thus not the stationary state observed typically in the long lived final metastable state. Moreover, the stationary state is now only a short-lived intermediate state, and it is determined by the model parameters, in particular by the value of w_0 which defines the depth of the detachment rate well. In this intermediate stationary stage, growth is determined essentially by the reaction kinetics. Although this stage is probably not easily detected by experiments, the model results suggest that it may be a typical intermediate stage of the evolution at low enough temperatures in case of 2D nanocluster growth.

The average size of the nanodots (as well as the maximum of the size distribution) depends clearly on the ambient temperature of the growth. The temperature dependence of the distribution shape is shown in Figure 5, and the detailed temperature dependence of the average size is shown in Figure 6. The temperature dependence is roughly of inverse power-law type $\langle s \rangle \propto (k_B T)^{-k}$ with values of k given in Figure 6. This strong temperature dependence can be traced back to the effect that the geometric factor s^q weights the Arrhenius-type reaction rates differently at different temperatures, thus making the detachment rate minimum shifting to larger sizes with decreasing temperature as shown in Figure 1. Therefore, from these results it is evident that the geometric capture rates affects also the properties of size distribution, as is expected if the stationary state is governed by growth kinetics in addition to the microscopic energetics of atomistic processes.

In summary, the present results agree with the results demonstrating the kinetically determined nature of the observed stationary state [12]. It should be noted that

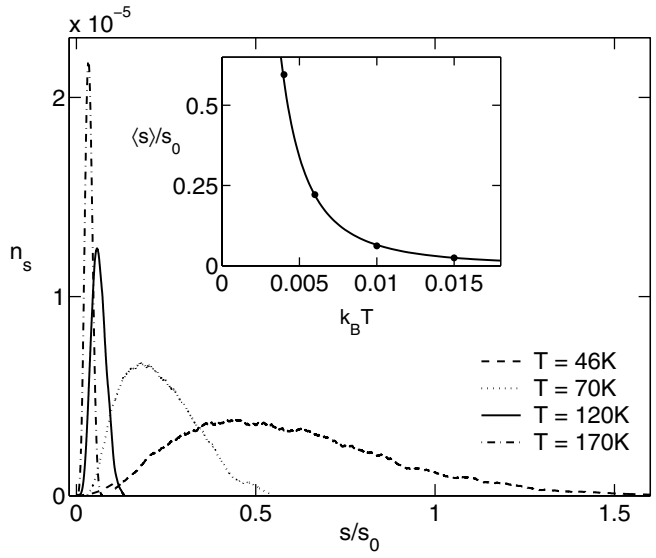

Fig. 5. The stationary size distributions n_s as a function of size s/s_0 at different temperatures in the intermediate stationary stage of growth. Note how the peaks move towards smaller sizes with increasing temperature. The distribution at 45 K is multiplied with the factor 100, at 70 K with 20 and at 120 K with 2. Parameter $q = 0.5$, others as in Figure 4. The inset shows the temperature dependence of mean size $\langle s\rangle/s_0$ of the distributions (dots) and the fit (compare with Fig. 6).

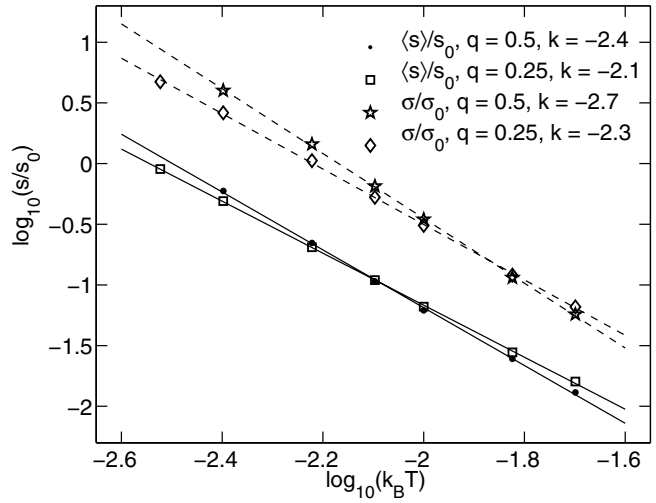

Fig. 6. The temperature dependence of the saturation size $\langle s\rangle/s_0$ (solid line) and the width σ/σ_0 (dashed line) at kinetically determined stationary stage of growth. The parameters are $t = 1.0 \times 10^7, \kappa = 1.0 \times 10^{-7}$, $c = 0.0002$ and $\alpha = 0.5$. Results for two different values of q are shown, with the slopes k for power-law fits. The error bars are smaller than the symbols.

the intermediate state is now obtained at quite low temperatures. This situation is simply related to the chosen parametrization, which is chosen to give the final stationary state at size region comparable to 2000–5000 atoms. With different parametrization, the temperature region may well be at considerably higher energies, but the then the final stationary stage of growth would occur at size region of 20 000–50 000 atoms, still feasible for our computational method but considerably slower. Also from computational aspect, it should be noted, that this intermediate stationary state may be quite long-lived in practice. The energetics parameter w_0 affects the lifetime of state by changing the depth of detachment rate minimum. Nevertheless, when the simulations are continued beyond the detachment minimum, the growth eventually starts again. In order to access the late stages of evolution it is essential to use the event-driven simulation methods like the BKL algorithm used in present work.

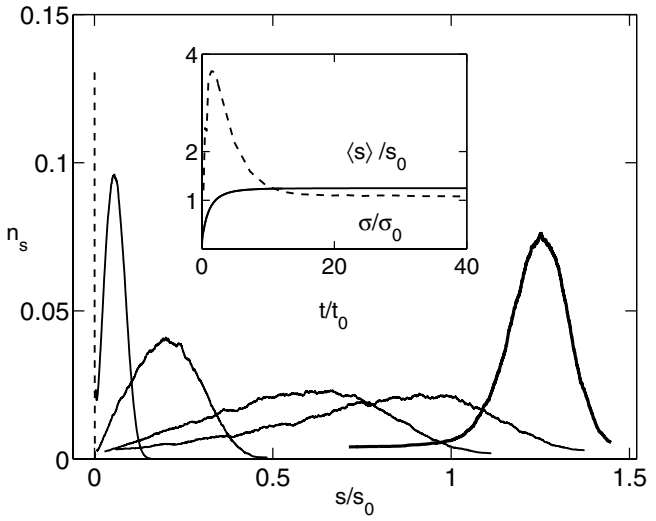

Fig. 7. The time development of size distributions n_s as a function of size s/s_0. The distributions are shown at times $2.0 \times 10^{-5}, 8.0 \times 10^3, 1.0 \times 10^5, 6.0 \times 10^5, 1.2 \times 10^6$ and 1.0×10^8 in arbitrary units, with $\kappa = 10^{-7}$ and temperature 350 K. For clarity: the distributions are multiplied with the factors 1, 2×10^4, 1×10^5, 4×10^5, 6×10^5, and 1×10^6, respectively. The initial singular distribution is marked with dashed line. In the inset are shown the average dot size $\langle s\rangle/s_0$ (solid line), and the standard deviation of the distribution σ/σ_0 (dashed line) as a function of time t/t_0. The size corresponding the energy minimum is $s_0 = 5000$ and $\sigma_0 \approx 350$ is the analytical estimate for the stationary width (see Appendix B).

3.3 Final stage of growth determined by energetics

When the growth continues beyond the kinetically determined stationary stage, the size-dependence of attachment rate begins to drive the growth again. The time development of the size distribution is shown in Figure 7. During this stage of growth, the size distribution begins to broaden rapidly. The front part of the distribution is Gaussian and propagates rapidly to larger sizes, while the trailing edge of the distribution is left behind and contains a large number of smaller dots. Consequently, distributions are skewed towards the small dot sizes. Finally, the width of distribution starts to diminish again and the distribution attains a closely Gaussian shape and becomes stationary. This stage of growth, where stationary state is approached, is extremely slow in comparison to initial and

intermediate stages of growth, as can be seen from the inset shown in Figure 7. The location of the stationary size does not depend on the temperature, but the width of the distribution is temperature dependent [4,14]. Therefore, in order to make better contact with previously discussed situations and experimental conditions where size selection is observed, we now discuss the results in temperature region which is higher than in the initial and intermediate cases.

In the final stationary state the average size (or the maximum of the distribution) is larger than the dot size s_0, which is the size for the minimum of free energy difference. The stationary size exceeds the value s_0 about a factor 1.3 in all cases studied here. This phenomenon of overshooting is determined by the balance of the distribution and the positive free energy gradient. Overshooting is clearly related to the kinetics of growth and is of similar origin as the kinetic overshooting effect studied by Jesson et al. [14]. As discussed in Appendix B, this condition is satisfied when the macroscopic mass current is $J = 0$ in the Fokker-Planck model describing the growth. This generally occurs only after the maximum of the distribution has passed over the minimum s_0 of the free energy difference (or in continuum model, the minimum of chemical potential). When this happens, the distribution begins to become narrower. The size distribution at the metastable state resembles in high degree the Gaussian distribution, but there are some differences. In order to quantify these differences we have calculated the variance of the distribution $\sigma^2 = [\sum_s (s - \langle s \rangle)^2 n_s)]/N$ and the suitably normalized third moment of the distribution, the skewness $\mu = [\sum_s ((s - \langle s \rangle)^3 n_s)]/[N\sigma^3]$ where $N = \sum_s n_s$.

The behaviour of the variance and skewness are shown in Figure 8. As is seen, the width changes in interesting way during growth, finally attaining a stationary value but first overshooting this stationary value by a factor of about 3–4. Similarly, the skewness of the distribution is first negative, signaling significant skewness towards small dots, but when the final long-lived stationary stage of growth is reached, it attains a small negative value. From the continuum approximation in Appendix B it is clear that the Gaussian distribution in stationary state needs to be slightly skewed. This originates from fulfilling the condition $J = 0$ at the size region where the free energy difference Δ_s has a positive gradient, in which case the distribution must have a compensating reduction in gradients.

Size selection observed in this final stage of growth is very general and generic process; it is produced with similar properties at least within values $\kappa = 10^{-1}$ to 10^{-8} if the product $\kappa t_{\max}$ is kept constant (here $t_{\max}$ is the maximum simulation time). Similarly, the changes in parameters defining the shape of the free energy of the system does not affect the basic qualitative features of the onset of the stationary state or the properties of the distribution. Of course, the absolute values of sizes where stationary state occurs do change, but the relative amount of the overshooting is always about 1.2–1.5 with different parameter combinations. For given values of q the skewness $|\mu|_c$

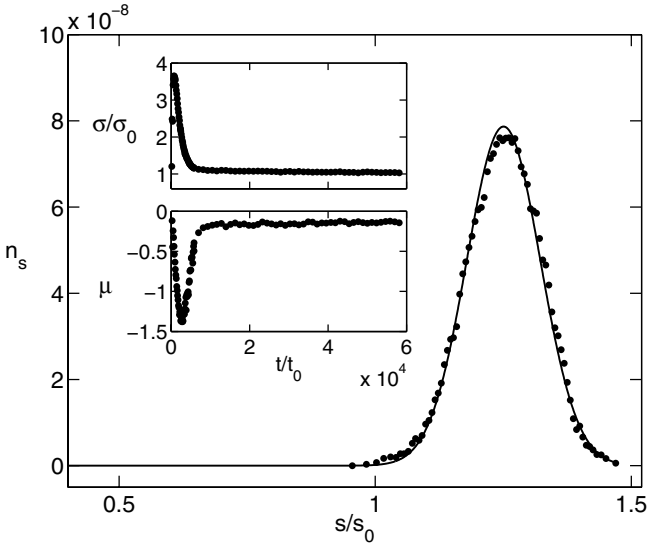

Fig. 8. The stationary size distribution n_s at the final metastable state ($t = 1.0 \times 10^8, \kappa = 1.0 \times 10^{-7}$, $c = 0.0002$, $\alpha = 0.5$ and temperature is 350 K). PCM simulations (dots) compared with the Gaussian distribution (solid line) calculated from the average size and the variance of data. Note the skewness of distribution compared to the Gaussian. Upper inset shows the time development of the standard deviation σ/σ_0. In the lower inset is the skewness μ of the size distribution as a function of time t/t_0. Parameters are $s_0 = 5000$, $\sigma_0 \approx 350$, and $t_0 \approx 1.7 \times 10^3$.

in the stationary state does not depend much on the choice of the other parameters and e.g. for $q = 1/2$ in the range $2.0 \times 10^{-4} < c < 2.0 \times 10^{-3}$ we found $|\mu|_c = 0.25$–0.33, while for $q = 1/4$ values $|\mu|_c = 0.5$–0.8 are obtained.

The skewness is connected to the effective driving force which causes the distribution to overshoot the value s_0. This can be seen in Figure 9, where the effective drift velocity ds/dt of the distribution peak is compared with the time evolution of skewness, and where the drift velocity is correlated with skewness at each instant of time in the region of growth where overshooting occurs. As is shown in Appendix B, the scaled, dimensionless drift velocity $|\bar{\mu}| = d(s/s_0)/d(t/t_0)$ at the position of maximum skewness, occurring in the vicinity of s_0, is estimated to be $|\bar{\mu}| = (\sigma_{max}/s_0)\,|\mu|_{max}$, where σ_{max} and $|\mu|_{max}$ are maximum values of distribution variance and skewness near s_0. In the cases studied here, this estimate predicts values of order $|\bar{\mu}| \approx 0.15$–0.20 which are in agreement with results shown in Figure 9. Moreover, it is possible to estimate the effect of the skewness on the magnitude of the overshooting within the Gaussian approximation (see Appendix B), and conclude that the final stationary size is $s_c \approx (1 + |\bar{\mu}|)s_0$. This estimate based on the Gaussian approximation is in concordance with the PCM simulation results, which give $s_c \approx 1.2 s_0$ in cases where $|\bar{\mu}| \approx 0.15$ and $s_c \approx 1.3 s_0$ when $|\bar{\mu}| \approx 0.20$. Similar variation between increasing overshooting with larger values of $|\bar{\mu}|$ are obtained in other cases.

The ambient temperature has mostly effect on the width of the distribution, as is shown in more detail in

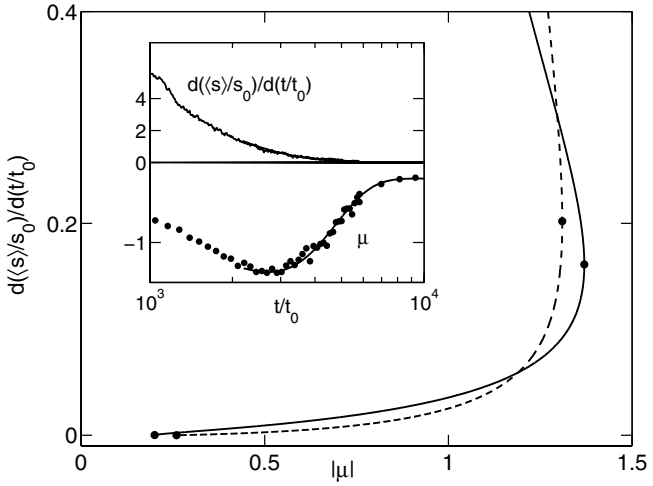

Fig. 9. The drift velocity of the average size $d(\langle s\rangle/s_0)/d(t/t_0)$ of the distribution as a function of the skewness μ with $\alpha = 0.5$ in solid line and $\alpha = 0.4$ in dashed line. The dots mark the turning points of curves and value at stationary state. Also the time dependences of the drift velocity and skewness (dotted, with solid line as fit) are shown in the inset. The distribution passes the minimum of free energy difference s_0 approximately at $t/t_0 = 1.2 \times 10^3$.

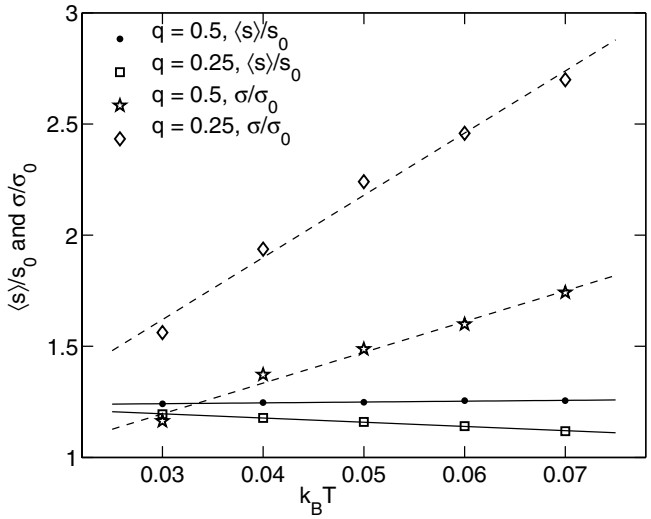

Fig. 10. The temperature dependence of the distribution peak position $\langle s\rangle/s_0$ (solid line) and the width of the distribution σ/σ_0 (dashed line). In the case shown, $s_0 = 5000$, $\sigma_0 \approx 350$, and other parameters are as in Figure 8. The errors are smaller than symbols.

Figure 10. The distribution broadens with the increasing temperature so that $\sigma \propto k_B T$, which is the relation predicted by the continuum approximation given in Appendix B [2,14]. However, also the average size in stationary state is affected by the temperature, but this is quite a moderate effect. In addition, the geometric attachment rate factor s^q affects the broadening, larger exponents q corresponding weaker temperature dependence as shown in Figure 10. The overall behaviour of the distributions is thus mainly determined by the energetics of the growth, but also affected by the kinetics. The results of PCM simulations, taken together with the fact that the distributions are Gaussian, confirms the prediction in reference [14] that due to interplay between energetics and kinetics of growth, a long-lived stationary or metastable state occurs.

4 Conclusions

We have discussed the the size selection of nanodots during their growth within the framework of reaction kinetic model. The theoretical formulation of the problem is based on the self-consistent reaction rates, where size dependent energetics is taken into account. The resulting model equations for the nanodot growth are solved by particle coalescence simulation method. The results show that during the growth there are three distinct stages of stationary growth and size selection. First, the initial stage of growth with anomalously high density of small dots, which can be described by simple continuum model with singular solutions. Second, there is a kinetically determined stationary stage of growth, which can be obtained if deposition is interrupted just after reaching the critical dot-size which defines the local maximum of the detachment rate. In this stage of the growth, the average size depends strongly on the temperature, the increasing temperature shifting distributions towards the smaller sizes. These regions of growth can be probably observed only at low enough growth temperatures. Third, there is a long-lived stationary state corresponding the minimum of the free energy difference (or chemical potential), and in this region selection of size occurs. In this stage of growth, kinetics still affects the growth by acting as an effective drift towards larger sizes, ultimately balanced by positive gradient of free energy difference (or chemical potential). Together these effects cause the peak position to overshoot the minimum and produce the small but essential skewness of size distributions in the stationary state. In this final stage, the width of the distribution is at the minimum, and is proportional to the temperature. The results suggest, that the final and long-lived stationary stage can be described with simple continuum models and with Gaussian solutions. However, the another kinetically determined precursor of short-lived stationary state with more complex properties does not seem to yield such simplified description. For further theoretical work the complete continuum description covering all the stages of the growth provides a challenging task.

This work has been supported by the the Academy of Finland through grant SA 1210516, the EU-project MagDot 661016 and through the Center of Excellence program by the Academy of Finland.

Appendix A

The problem of defining the reaction rates for attachment and detachment for reversible nucleation and growth in epitaxial growth has been discussed within the framework of the self-consistent rate theory by Bales and Zangwill [23]. The basic question is how to take into account the effect of additional barriers for attachment (or alternatively, lowered barrier for detachment) of adatoms on the edges of the 2D-clusters. Basically, the additional barrier modifies the adatom density on the dot edge, and these modifications caused by the reversible nature of growth must be taken onto account on the reaction rates themselves. In the approach suggested by Bales and Zangwill the adatom density around the dot is solved by using the boundary condition on the dot edge which takes into account that: (1) the rate of detachment ω_s from the edge of the cluster of size s is different from the rate γ_s at which the adatoms can escape to the surrounding medium consisting of adatoms; (2) the effective rate γ_s depends on the concentration of adatoms on the cluster edge, and in equilibrium this concentration is increased by detachment, and thus related to the additional barrier Δ_s for attachment (or lowered barrier for detachment). This situation requires that the rates of attachment and detachment are calculated self consistently, so that "bare" detachment rate ω_s from cluster edge with radius R_s is modified by the re-adsorption effect. In the model by Bales and Zangwill, the re-adsorption is assumed to be possible through several pathways m_s, which for large clusters is $m_s \to 2\pi R_s$ (in what follows, we use units scaled with lattice constant a, so that in comparison to Bales and Zangwill we have always $a = 1$). The self consistent scheme leads to the result that attachment rate (capture rate) σ_s and the corresponding detachment rate $\gamma_s = 1/\tau_s$, where τ_s is escape time, can be chosen to be (see Eqs. (18) and (19) in Ref. [23])

$$\sigma_s = \frac{2\pi R_s K_1(R_s/\xi)}{\beta_s^{-1} K_1(R_s/\xi) + \xi K_0(R_s/\xi)} \tag{A.1}$$

$$\gamma_s = \frac{\omega_s \sigma_{s-1}}{m_{s-1} e^{-\Delta_{s-1}/k_B T}} \tag{A.2}$$

where $\beta_s^{-1} = (2\pi R_s/m_s)e^{\Delta_s/K_B T} - 1$, and K_0 and K_1 are modified Bessel functions of the second kind of order 0 and 1, respectively. In this form, all effects of detachment are taken into account and rate γ_s becomes now the effective rate at which detached adatoms escape into the medium consisting of adatoms (effective medium) on which the clusters are embedded [23]. In these equations, the parameter ξ (for definition, see Ref. [23] Eq. (6) and Ref. [30] Eq. (13)) is the correlation length, i.e. the average length the adatom travels before being captured by a cluster edge. It should be noted, that in our point-like dot model based on the RKM this correlation length is a free parameter, defining the density of the system.

The detailed forms of the self-consistent rates are still too complicated and detailed for our purposes. In order to simplify the reaction rates further we assume that $2\pi R_s/m_s = 1$, and that $\xi K_0(x)/K_1(x) = 1$. Of these assumptions, the latter is more restrictive, and it confines the approximation to be used in region where radius of dots is small in comparison to correlation length and correlation length is in principle large. This is consistent with assumptions of the point-like dot model behind RKM, although it should be noted that in point-like dot model it can not be defined unambiguously. In practice, the choice of ξ and ratio $K_0(x)/K_1(x)$ does not affect in any significant way the evolution of the system, because it mostly defines the saddle point of rates seen in Figure 1 (related to the size of islands up to which initial, singular evolution continues), but its effect on the exact location of the saddle point is quite moderate. In addition, the "bare" detachment rate is taken to be a simple power-law $\omega_s = s^q$. With these simplifications we obtain

$$\begin{aligned} \sigma_s &= s^q/(1 + e^{\beta\Delta_s}); \\ \gamma_s &= s^q/(1 + e^{-\beta\Delta_{s-1}}), \end{aligned} \tag{A.3}$$

which are mathematically simple enough but still retain the essential physics for our purpose of exploring the qualitative and generic features of the RKM model.

Appendix B

The reaction kinetic model (RKM) defined by equations (1–4) can be simplified further for analytical calculations. The first step is deriving the discrete Becker-Döring model (BDM) from the RKM, and then from the BDM a generalized Fokker-Planck model (FPM), which is a continuum model for growth.

B.1 The Becker-Döring model

The basic physical assumptions behind the RKM are the assumptions of steady diffusion, total mass conservation and isolated dots in a dilute system, and these are similarly the starting point for classical derivations of Becker-Döring model (see Ref. [31] and references therein). In order to see how RKM defined by REs in equation (1) are related to the BDM we first note that the regular growth takes place when $dn_1/dt \to 0$ and this requires that $n_1 \to \kappa$. Second, by using the value $n_1 = \kappa$ and redefining $n_1 \to n_1/\kappa$ equation (1) is simplified to the Becker-Döring model defined by equations [31]

$$\begin{aligned} \frac{dn_s}{dt} &= \sigma_{s-1} n_{s-1} - (\sigma_s + \gamma_s) n_s + \gamma_{s+1} n_{s+1} \\ &\quad + \eta(\sigma_s n_s - \gamma_{s-1} n_{s-1}), \end{aligned} \tag{B.1}$$

where the parameter $\eta = n_1 - 1$ is a measure for deviation of the adatom density. In what follows, we assume that growth is completely regular (i.e. $n_1 = \kappa$), when $\eta = 0$. This assumption is consistent with the growth condition corresponding either the existence of a wetting layer, the super-saturation of adatoms [5] or enhanced detachment of adatoms from cluster edges [17,18]. In what follows, we

assume a constant pre-deposited coverage θ, and that the adatom density is supersaturated (or that a wetting layer exists), justifying the condition $\eta = 0$.

B.2 The Fokker-Planck model

The Becker-Döring model in equation (B.1) describes the growth in atomistic level through reaction rates [31]. The corresponding continuum equation for evolution of the size distribution $n(x,t)$ for size x treated as a continuous variable can be derived by performing the Kramers-Moyal expansion [32] of the Becker-Döring model. This expansion leads to Fokker-Planck model given by equations (compare with [14])

$$\frac{\partial n(x,t)}{\partial t} = -\frac{\partial}{\partial x}[J(x,t)], \tag{B.2}$$

$$J(x,t) = v(x,t)n(x,t) - \frac{\partial}{\partial x}[D(x,t)n(x,t)], \tag{B.3}$$

where $J(x,t)$ is the flux in configurational space of dot sizes. The time and size dependent drift and diffusion coefficients are given by

$$v(x,t) = x^q \tanh\left[\frac{\Delta(x)}{2k_BT}\right], \tag{B.4}$$

$$D(x,t) = \frac{1}{2}x^q. \tag{B.5}$$

In deriving equation (B.5) we have made the assumption that $\xi K_0(x)/K_1(x) = 1$ (see Appendix A, from Eqs. (A.2) to (A.3)). This assumption does not affect the evolution of the system in the region $x > 0.2x_0$ where the curvature of $\Delta(x)$ near its minimum x_0 dominates the growth. In addition, we approximate $\tanh[\Delta/2k_BT] \to \Delta\beta/2$, and make the scaling $t \to t/2$.

B.3 Initial evolution and singular distributions

The initial stage of growth or at temperatures where $\beta\Delta_s \ll 1$ the FPE can be approximated by neglecting the drift term, in which case equation (B.2) reduces to

$$\frac{\partial n(x,t)}{\partial t} = \frac{\partial^2}{\partial x^2}[x^q n(x,t)]. \tag{B.6}$$

This non-linear diffusion equation has solutions [33]

$$n(x,t) \propto x^{-q} \exp\left[-\frac{x^{2-q}}{(2-q)^2 t}\right], \tag{B.7}$$

and with respect to the spatial scales it has a scaling property $x \to x/t^\beta$ (for details, see from Eq. (1) to Eq. (10) in Ref. [33]), where the dynamic exponent is given by

$$\beta = 1/(2-q). \tag{B.8}$$

The results of the PCM simulations shown in Figure 3 are in concordance with this kind of initial stage with the size distribution having a characteristic singularity $n(x) \propto x^{-q}$ at small values of x. However, in cases studied here this growth stage is too short in order to show clearly the dynamic scaling and scaling of singular distributions.

B.4 Stationary state and Gaussian distributions

The Fokker-Planck equations in equations (B.2, B.3) have previously been used to describe the growth of nanodots in stationary stage of growth by Jesson et al. [14]. In the region, where the minimum of the energy change $\Delta(x)$, or alternatively in the continuum limit the minimum of chemical potential, governs the growth of the nanodots it is possible to obtain a long-lived stationary state of growth. The numerical results in reference [14] show that the time evolution of the size distribution is rather regular: the distribution is already from the beginning a Gaussian-shaped and evolves steadily towards the metastable state, which is long-lived. Already before this long-lived metastable state is reached, the width of the size distribution begins to diminish until finally a stationary state is obtained and the the average size remains the same. This behaviour suggests that it is possible to find simple solutions to the Fokker-Planck model describing the growth, and to use such solutions in describing the effect of overshooting the size corresponding the free energy minimum as well as the narrowing of the distribution.

In the long-lived stationary (or metastable) region of growth a reasonable assumption is that the distribution is sufficiently narrow so that the energy difference $\Delta(x)$ (or the chemical potential) can be linearized in the vicinity of the size distribution maximum $\bar{x}$, in which case $\Delta(x) \approx \Delta(\bar{x}) + \Delta'(\bar{x})(x-\bar{x}) + (1/2)\Delta''(\bar{x})(x-\bar{x})^2$. This assumption, which greatly simplifies the description of the growth problem, can be justified a posteriori (see also [14]). However, now we must ensure the conservation of the mass and thus require that the total flux after approximations satisfies

$$\int_0^\infty J(x,t)dx = 0. \tag{B.9}$$

This requires that an average energy change $\bar{\Delta}$ (a Lagrange multiplier) to take care of the mass conservation is introduced so that the drift velocity is given by

$$v(\bar{x},t) = \beta D(x)[\bar{\Delta} - \Delta(x)] - \beta D(x)\Delta'(x)[\bar{x} - x], \tag{B.10}$$

where the diffusion coefficient is $D(x) = x^q$, and $\bar{\Delta}$ depends only on time through the condition in equation (B.9). We assume that the size distribution is sharply enough peaked around $x = \bar{x}$ to allow the approximation $D(x) = D(\bar{x})$, $\Delta(x) = \Delta(\bar{x})$ and $\Delta'(x) = \Delta'(\bar{x})$ throughout all further calculations (in what follows, the argument $\bar{x}$ is dropped out from these coefficients). In this case the simplified FPM has a drift velocity which depends linearly on the position x but the terms D, Δ and Δ' depend only on time through the time dependence of the size $\bar{x}$.

The FPM defined by equations (B.2, B.3) and equation (B.10) is now reduced to the Fokker-Planck model with time dependent diffusion and linearized drift. This kind of FPM can be solved by a Gaussian-distribution

$$n_G(x,t) = \frac{1}{\sqrt{2\pi\sigma^2}} \exp\left[-\frac{(x-\bar{x})^2}{2\sigma^2}\right], \tag{B.11}$$

with the time-dependent peak position $\bar{x} = \bar{x}(t)$ and the distribution width (standard deviation) $\sigma = \sigma(t)$ [34,35]. In principle, the integral transforms for calculating $\bar{x}$ and σ are given e.g. in references [34,35], but now it is more convenient to use the differential equations defining the average size $\bar{x}$ and the standard deviation $w = \sigma^2$ of the distribution:

$$\frac{d\bar{x}}{dt} = \beta D(\bar{\Delta} - \Delta) - \beta D\Delta'(\bar{x} - x_0), \qquad \text{(B.12)}$$

$$\frac{dw}{dt} = 2D - 2\beta\, D\, \Delta' w. \qquad \text{(B.13)}$$

The major complication with equations (B.12, B.13) arises from the notion that $\bar{\Delta}$ is time dependent. However, as a first approximation we note that difference $\bar{\Delta} - \Delta$ can be interpreted as an effective drift. In the vicinity of $\bar{x} = x_0$ only this part of the effective drift affects the time development of the peak position as is seen from equation (B.12). Moreover, as is shown in Figure 9, the PCM simulations show that for $x > x_0$ there is a correlated decrease of skewness and the drift velocity. This dependence suggests that on the average the effective constant drift $\bar{\Delta} - \Delta$ can be related to the skewness μ of the distribution. Within the simplified model it is not possible to make this relationship entirely quantitative, but it is possible to approximately relate $\bar{\Delta} - \Delta$ to the skewness μ by deriving the time rate of change of the third moment of the distribution and assuming then its stationarity. For values of x close to the stationary size $x_c > x_0$ we obtain then an estimate

$$\bar{\Delta} - \Delta \approx |\mu|_{max}\ \langle \sigma/x_0 \rangle_{max}\, \Delta'\, x_0. \qquad \text{(B.14)}$$

Therefore, after the distribution has passed the position x_0 the drift speed is $d\bar{x}/dt = v_0|\bar{\mu}|$, where $v_0 = x_0/t_0$ with a timescale factor $t_0 = [\beta D(x_0)\Delta'(x_c)]^{-1}$. Defining $|\bar{\mu}| = |\mu|_{max} \langle \sigma/x_0 \rangle_{max}$ and taking into account that PCM simulations give values $1.5 < |\mu|_{max} < 2.0$ and $0.2 < \langle \sigma/x_0 \rangle_{max} < 0.3$ we obtain $0.2 < |\bar{\mu}| < 0.3$ for $q = 1/2$ and $0.3 < |\bar{\mu}| < 0.5$ for $q = 1/4$. These estimates are in agreement with drift velocities inferred from the PCM data, which for $q = 1/2$ and $1/4$ (for a range of other parameters) give $(d\bar{x}/dt)/v_0 \approx 0.16$–$0.20$ and 0.25–0.30, respectively.

The final simplification occurs when the result in equation (B.14) is substituted in equations (B.12, B.13). We define the scaled variables as $\tau = t/t_0$, $\zeta = \bar{x}/x_0$, and scaled functions as $\omega = \sigma^2/\sigma_c^2$ and $\tilde{\Delta}'(\zeta) = \Delta'(x)/\Delta'(x_c)$, where $\sigma_c^2 = 1/(\beta\Delta'(x_c))$ is the width at the stationary position x_c. With these redefinitions we obtain

$$\dot{\zeta} = (1 + |\bar{\mu}|) - \zeta, \qquad \text{(B.15)}$$

$$\dot{\omega} = 2 - 2\tilde{\Delta}'(\zeta)\, \omega. \qquad \text{(B.16)}$$

Within the present model, we do not have access to calculate the values of the parameter $|\bar{\mu}|$, which need to be obtained from simulations. In most cases $0.2 < |\bar{\mu}| < 0.5$ can be used as rough estimates. The quantitative accuracy of the simplified model can not be improved further, but these estimates are enough to demonstrate the origin of the overshooting effect. The time evolution of the scaled average size ζ and width ω is now calculated easily from equations (B.15) and (B.16). The only complication is that $\tilde{\Delta}'(\zeta)$ is singular at small values of ζ. However, in this region our basic linearization assumption fails, and without any additional loss of reliability $\tilde{\Delta}'(\zeta)$ can be replaced by suitably smooth approximating function at values $\zeta < 0.5$. This only affects the behaviour of ω at the region where it reached maximum. Some results for different choices of model parameters are shown in Figure 11, where the typical behaviour comparable to behaviour seen in PCM calculations (see the inset in Fig. 7) is demonstrated.

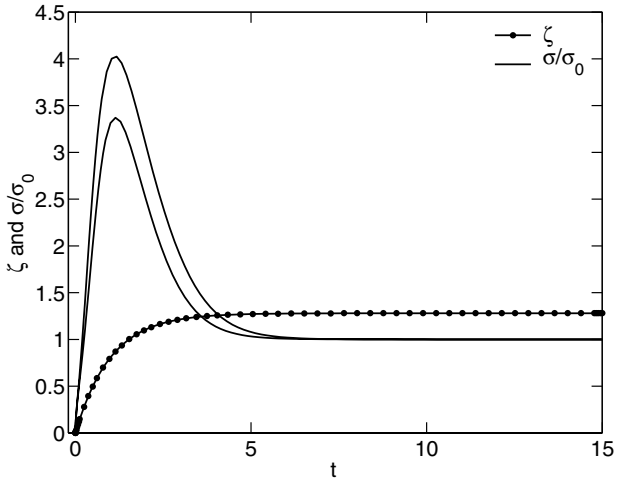

Fig. 11. The time evolution of the the scaled average size ζ and the width σ/σ_c for different approximations of $\tilde{\Delta}'(\zeta)$. Compare with the corresponding PCM results in the inset of Figure 7.

From these results, it can be seen that the stationary values are simply obtained as $\zeta_c = 1 + |\bar{\mu}|$ and $\omega_c = 1$, corresponding the stationary average size x_c and width σ_c given by

$$x_c = (1 + |\bar{\mu}|)\, x_0, \qquad \text{(B.17)}$$

$$\sigma_c = 1/\sqrt{\beta\Delta'(x_c)}. \qquad \text{(B.18)}$$

Therefore, x_c overshoots x_0 by a fraction depending of $|\bar{\mu}|$, as well as the width of the distribution increases up to s_0 after it starts to decrease rapidly towards the stationary value determined by $\sigma_c = 1/\sqrt{\beta\Delta_c'}$. These predictions compare well with the results of PCM simulations. In addition, the behaviour of distribution based on the linearized form of free energy in the vicinity of the average size is in agreement with the results in reference [14], where linearization is not done. However, the fact that also in their case Gaussian distributions are obtained strongly suggests that distributions are narrow enough to justify the linearization. This notion is also supported by the results of our RKM model. Given the simplicity of the scheme proposed here and the agreement with results based on the RKM and the direct numerical solution of the Fokker-Planck model, the sacrifice of accuracy due to the linearization of drift appears to be tolerable.

References

1. D.J. Eaglesham, M. Cerullo, Phys. Rev. Lett. **64**, 1943 (1990)
2. C. Priester, M. Lannoo, Phys. Rev. Lett. **75**, 93 (1995)
3. M. Kobayashi, T.M. Ramachandran, P. Chen, A. Madhukar, Appl. Phys. Lett. **68**, 3299 (1996)
4. D. Leonard, K. Pond, P.M. Petroff, Phys. Rev. B **50**, 11687 (1994)
5. F. Liu, A.H. Li, M.G. Lagally, Phys. Rev. Lett. **87**, 126103 (2001)
6. Z. Gai, B. Wu, G.A. Farnan, D. Shu, M. Wang, Z. Zhang, J. Shen, Phys. Rev. Lett. **89**, 235502 (2002)
7. F. Rosei, J. Phys.: Condens. Matter **16**, S1373 (2004)
8. F. Patella, A. Sgarlata, F. Arciprete, S. Nufris, P.D. Szkutnik, E. Placidi, M. Fanfoni, N. Motta, A. Balzaroti, J. Phys. Condens. Matter **16**, S1503 (2004)
9. F. Liu, Phys. Rev. Lett. **89**, 246105 (2002)
10. J. Shen, J.P. Pierce, E.W. Plummer, J. Kirschner, J. Phys. Condens. Matter **15**, R1 (2003)
11. F. Komori, S. Ohno, K. Nakatsuji, J. Phys. Condens. Matter **14**, 8177 (2002)
12. M. Meixner, E. Schöll, V.A. Shchukin, D. Bimberg, Phys. Rev. Lett. **87**, 236101 (2001)
13. M. Meixner, R. Kunert, E. Schöll, Phys. Rev. B **67**, 195301 (2003)
14. D.E. Jesson, T.P. Munt, V.A. Shchukin, D. Bimberg, Phys. Rev. Lett. **92**, 115503 (2004)
15. V.A. Shchukin, D. Bimberg, Rev. Mod. Phys. **71**, 1125 (1999)
16. R.E. Rudd, G.A.D. Briggs, A.P. Sutton, G. Medeiros-Ribeiro, R.S. Williams, Phys. Rev. Lett. **90**, 146101 (2003)
17. H.T. Dobbs, D.D. Vvedensky, A. Zangwill, J. Johansson, N. Carlsson, W. Seifert, Phys. Rev. Lett. **79**, 897 (1997)
18. H.M. Koduvely, A. Zangwill, Phys. Rev. B **60**, R2204 (1999)
19. M. Rusanen, I.T. Koponen, J. Asikainen, Eur. Phys. J. B **36**, 567 (2003); I.T. Koponen, M.O. Jahma, M. Rusanen, T. Ala-Nissilä, Phys. Rev. Lett. **92**, 086103 (2004)
20. D. Turnbull, J.C. Fisher, J. Chem. Phys. **17**, 71 (1949)
21. K.F. Kelton, A.L. Greer, Phys. Rev. B **38**, 10089 (1988)
22. A. Ziabicki, L. Jarecki, J. Chem. Phys. **80**, 5751 (1984)
23. G.S. Bales, A. Zangwill, Phys. Rev. B **55**, R1973 (1997)
24. J. Tersoff, R.M. Tromp, Phys. Rev. Lett. **70**, 2782 (1993); F.M. Ross, J. Tersoff, R.M. Tromp, Phys. Rev. Lett. **80**, 984 (1998)
25. R. Bahadur, R.B. McClurg, J. Chem. Phys. **121**, 12499 (2004)
26. A. Lo, R.T. Skodje, J. Chem. Phys. **112**, 1966 (2000)
27. P.L. Krapivsky, J.F.F. Mendes, S. Redner, Eur. Phys. J. B **4**, 401 (1998); P.L. Krapivsky, J.F.F. Mendes, S. Redner, Phys. Rev. B **59**, 15950 (1999)
28. K. Kang, S. Redner, Phys. Rev. A **30**, 2833 (1984); K. Kang, S. Redner, Phys. Rev. Lett. **52**, 955 (1984); K. Kang, S. Redner, P. Meakin, F. Leyvraz, K. Kang, S. Redner, Phys. Rev. A **33**, 1171 (1986)
29. A.B. Bortz, M.H. Kalos, J.L. Lebowitz, J. Comp. Phys. **17**, 10 (1975)
30. G.S. Bales, D.C. Chrzan, Phys. Rev. B **50**, 6057 (1994); J.G. Amar, M.N. Popescu, F. Family, Phys. Rev. Lett. **86**, 3092 (2001); J.W. Evans, M.C. Bartelt, Phys. Rev. B **63**, 235408 (2001)
31. J.J.L. Velázquez, J. Stat. Phys. **92**, 195 (1998)
32. H. Risken, *The Fokker-Planck Equation* (Springer, Berlin, 1984)
33. K.S. Fa, E.K. Lenzi, Phys. Rev. E **67**, 061105 (2003)
34. F. Benamira, L. Guechi, Europhys. Lett. **56**, 8 (2001)
35. C.F. Lo, Europhys. Lett. **39**, 263 (1997); P. Demo, A.M. Sveshnikov, Z. Kožíšek, Europhys. Lett. **50**, 278 (2000)